Food Control 184 (2026) 112033

Contents lists available at ScienceDirect

Food Control

journal homepage: www.elsevier.com/locate/foodcont

Detection of deoxynivalenol, its modified forms, and zearalenone in individual oat grains using visible-near-infrared spectroscopy and near-infrared hyperspectral imaging

Irene Teixido-Orries [a], Francisco Molino [a,*], Carol Verheecke-Vaessen [b], Angel Medina [b], Sonia Marín [a]

[a] Applied Mycology Unit, Department of Food Technology, Engineering and Science, University of Lleida, AGROTECNIO-CERCA Centre, Av. Rovira Roure 191, 25198, Lleida, Spain
[b] Magan Centre of Applied Mycology, Cranfield University, Cranfield MK43 0AL, United Kingdom

ARTICLE INFO

Keywords:
Applied mycology
Deoxynivalenol
Modified forms
Zearalenone
Near-infrared
Visible range
Spectroscopy

ABSTRACT

Fusarium mycotoxins such as deoxynivalenol (DON), its modified forms, and zearalenone (ZEN) frequently contaminate oats, posing serious health and regulatory concerns. This study assessed the use of visible-near-infrared (Vis-NIR) spectroscopy and near-infrared hyperspectral imaging (NIR-HSI) to classify individual oat grains according to the European legal limits for DON (1750 μg/kg) and ZEN (100 μg/kg). NIR-HSI consistently outperformed Vis-NIR, achieving classification accuracies (CAs) above 91% and F1-scores above 0.65 for DON, ZEN and combined DON + ZEN detection. The most informative spectral regions were in the NIR ranges of 1000-1250 nm and 1300-1500 nm, associated with *Fusarium*-induced biochemical and structural changes in oat grains. Reducing the spectral input to 20 selected wavelengths preserved NIR-HSI performance, supporting the feasibility of multispectral implementations. These targeted, non-destructive approaches could enable early removal of the few highly contaminated grains responsible for batch rejection, improving food safety, reducing waste, and enhancing the sustainability of oat processing.

1. Introduction

Oats (*Avena sativa* L.) are increasingly recognised as a functional cereal crop due to their high content of soluble dietary fibre, particularly β-glucans, which have been shown to reduce serum cholesterol and support cardiovascular health (Paudel et al., 2021). These nutritional attributes, along with growing consumer interest in plant-based and fibre-rich foods, have led to an expansion of oat production and consumption worldwide (Yang et al., 2023). However, like other small-grain cereals, oats are susceptible to infection by *Fusarium species*, especially *F. graminearum* and *F. culmorum*, which can lead to the accumulation of mycotoxins such as deoxynivalenol (DON) and zearalenone (ZEN) (Hofgaard et al., 2016; Tarazona et al., 2021). These mycotoxins pose significant risks to human and animal health (Bezerra da Rocha et al., 2014). DON, a type B trichothecene, is associated with nausea, vomiting, impaired intestinal function, and immune suppression. However, ZEN can disrupt hormonal balance and affect reproductive health due to its oestrogenic activity (Ekwomadu et al., 2021). As a result, both compounds are regulated in the European Union (EU), with maximum limits for unprocessed oats set at 1750 μg/kg for DON and 100 μg/kg for ZEN (European Commission, 2023b, 2024a).

The challenge extends beyond these free forms. Several modified forms of DON, including 3-acetyldeoxynivalenol (3-ADON), 15-acetyldeoxynivalenol (15-ADON), and deoxynivalenol-3-glucoside (DON-3G), are also commonly present in oats (Meyer et al., 2021). While not currently regulated, these compounds are toxicologically relevant and often go undetected in routine analyses (Rychlik et al., 2014). Thus, the European Commission (2024a) has highlighted the importance of considering not only the content of DON but also the sum of DON, 3-ADON, 15-ADON, and DON-3G to assess human health risk. Critically, these modified forms show strong correlations with DON in naturally contaminated oats, with reported correlation coefficients typically exceeding 0.90 (Nathanail et al., 2015). In addition, DON and ZEN also tend to co-occur, although the correlation is generally lower; for example, a correlation coefficient of 0.52 was observed in a study of European oat samples (Fredlund et al., 2013). This means that grains with high DON levels often contain high concentrations of DON-3G,

* Corresponding author.
E-mail address: francisco.molino@udl.cat (F. Molino).

https://doi.org/10.1016/j.foodcont.2026.112033
Received 6 November 2025; Received in revised form 15 January 2026; Accepted 3 February 2026
Available online 3 February 2026
0956-7135/© 2026 The Authors. Published by Elsevier Ltd. This is an open access article under the CC BY-NC license (http://creativecommons.org/licenses/by-nc/4.0/).

Nomenclature

3-ADON	3-acetyldeoxynivalenol
15-ADON	15-acetyldeoxynivalenol
AUC	Area under the receiver operating characteristic curve
CA	Classification accuracy
DON	Deoxynivalenol
DON-3G	Deoxynivalenol-3-glucoside
ESI	Electrospray ionisation
ELISA	Enzyme-linked immunosorbent assay
EU	European Union
HPLC	High-performance liquid chromatography
HSI	Hyperspectral imaging
LC-MS/MS	Liquid chromatography-tandem mass spectrometry
LDA	Linear discriminant analysis
LFD	Lateral flow devices
LOD	Limit of detection
LOQ	Limit of quantification
MRM	Multiple reaction monitoring
MS	Mass spectrometry
NIR	Near-infrared
PCA	Principal component analysis
PLS	Partial least squares
R2	Determination coefficient
ROC	Receiver operating characteristic
RSD	Relative standard deviation
SD	Standard deviation
SNV	Standard normal variate
Vis	Visible range
ZEN	Zearalenone

3-ADON, and 15-ADON, and may also contain ZEN.

Mycotoxin contamination in oats is typically heterogeneous, with most grains being either clean or lightly contaminated, and only a small proportion containing high concentrations (Blackshaw-Crosby, 2021). These few heavily contaminated grains can push the average contamination of a batch above regulatory thresholds, resulting in food waste and economic losses. Identifying and removing these grains early in the processing chain could significantly reduce the carry-over of mycotoxins into final food products, helping to safeguard both food safety and product quality (Dropa et al., 2021).

Conventional detection methods such as high-performance liquid chromatography (HPLC), liquid chromatography-tandem mass spectrometry (LC-MS/MS), lateral flow devices (LFD), and enzyme-linked immunosorbent assays (ELISA) are normally used in the food industry entry point to analyse DON and ZEN in batch samples (Maphaisa et al., 2025). However, these methods are usually performed on bulk samples that may not reflect contamination levels in individual grains, and they can also be expensive, destructive, and unsuited to high-throughput, real-time screening (Krska et al., 2014). In contrast, visible-near-infrared (Vis-NIR) spectroscopy and near-infrared hyperspectral imaging (NIR-HSI) offer fast, non-destructive analysis and have shown potential for detecting DON and other mycotoxins in cereals (Femenias et al., 2020; Zareef et al., 2021). These techniques allow the chemical and physical characterisation of grains without sample preparation (Femenias, Gatius, et al., 2022). In contrast to bulk mycotoxin screening, spectroscopy can also be applied at the level of individual grains, enabling the analysis of spectral variability within a batch and the identification of highly contaminated units (Freitag, 2025). Single-grain NIR analysis is not a new concept and has been explored since the 1980s; notably, the first report of mycotoxin identification at the level of an individual cereal kernel was published in 1980, as reviewed by Chavez et al. (2020). By analysing grains individually, spectroscopic approaches at the single-grain level enable the detection of extreme contamination events that may be masked in bulk analyses, which is particularly relevant for mycotoxins characterised by highly heterogeneous distributions.

Importantly, advances in instrumentation and data processing have enabled the translation of this concept into industrial practice. Commercial NIR-based optical sorters are currently available and capable of analysing and classifying thousands of grains per second in real time (Taylor & Newkirk, 2023). These systems have already been implemented in cereal processing chains and shown to reduce mycotoxin contamination in accepted fractions by selectively removing defective or highly contaminated grains. As such, single-grain NIR analysis represents a practical bridge between laboratory-scale detection and industrial-scale mitigation strategies.

Although recent studies have demonstrated their feasibility for DON and T-2 and HT-2 toxins in oat samples, most have focused on bulk analysis (Teixido-Orries, Molino, Femenias, et al., 2023; Teixido-Orries, Molino, Gatius, et al., 2023; Tekle et al., 2013). Tekle et al. (2015) developed classification models for individual oat grains using NIR-HSI to classify individual pixels of artificially contaminated oats based on *Fusarium* damage and DON content. Moreover, in our previous study, T-2 and HT-2 toxins were detected in individual oat grains at levels above or below the legal limit using Vis-NIR and NIR-HSI spectroscopy (Teixido-Orries et al., 2026). However, applications to naturally contaminated grains remain scarce, even though targeting these grains could enable simultaneous removal of multiple mycotoxins. Given the strong correlations among DON and its derivatives, removing DON-contaminated grains would also reduce levels of DON-3G, 3-ADON, and 15-ADON, and may also reduce ZEN content. To date, the detection of ZEN and DON-modified forms in cereals using Vis-NIR spectroscopy or NIR-HSI has not been reported. This can represent a highly efficient mitigation strategy by reducing the risk of rejecting uncontaminated batches or accepting contaminated ones. In turn, such an approach could help maintain lower mycotoxin levels in the accepted fraction, thereby enhancing food safety and regulatory compliance, while also improving the economic efficiency and sustainability of oat production by reducing food losses and the financial burden associated with batch rejection.

For industrial development, however, simplified models are necessary. Full-spectrum spectroscopic models are computationally intensive and not practical for real-time sorting systems. By identifying and selecting a limited number of informative wavelengths, multispectral models can be developed that are faster, more robust, and easier to implement in automated grain processing lines (Wan et al., 2020).

Therefore, this study aims to evaluate the potential of Vis-NIR and NIR-HSI spectroscopy for detecting individual oat grains contaminated with DON and its modified forms (DON-3G, 3-ADON, 15-ADON), as well as ZEN, using LC-MS/MS as a reference method. These grains come from samples with DON levels above the EU legal limit. The specific objectives are to develop classification models capable of identifying grains exceeding EU legal thresholds for DON and/or ZEN, explore the spectral features associated with contamination, and reduce model complexity through wavelength selection.

2. Materials and methods

2.1. Oat samples

Two samples of white unprocessed oat grains (*Avena sativa* L.) were selected based on their high DON concentration. These were collected in the Västra Götaland region (Sweden) during the 2021 season. Sample 1 had 3184 μg/kg of DON, 851.0 μg/kg of DON-3G, 98.6 μg/kg of 15-

ADON, 268.2 μg/kg of 3-ADON, and 55.7 μg/kg of ZEN. Sample 2 had 3813 μg/kg of DON, 851.8 μg/kg of DON-3G, 111.7 μg/kg of 15-ADON, 288.4 μg/kg of 3-ADON, and 48.7 μg/kg of ZEN. From each sample, 100 individual grains were randomly selected, resulting in a total of 200 oat grains analysed in this study as described in Section 2.5.

2.2. Chemicals and reagents

All mycotoxin reference standards were purchased from Romer Lab (Tulln, Austria) and prepared in acetonitrile. The working concentrations were as follows: DON (100 μg/mL), DON-3G (50.1 μg/mL), 3-ADON (100 μg/mL), 15-ADON (100.2 μg/mL), and ZEN (100 μg/mL).

Ultrapure water was produced using a PURELAB® Chorus 1 system (ELGA LabWater, Buckinghamshire, UK). Ammonium acetate (>99%, analytical grade), glacial acetic acid (99.7%, HPLC grade), methanol (LC–MS grade), and acetonitrile (LC–MS grade) were obtained from Fisher Scientific (Waltham, MA, USA).

2.3. NIR-HSI experimental work: instrumentation and data acquisition

A push-broom hyperspectral imaging system composed of a Pika NIR-320 camera assembled by Resonon Inc. (Bozeman, MA, USA) was used (Fig. 1A). The device consists of an InGaAs sensor line-scan camera with a 320 × 256-pixel resolution, a 14-bit A/D spectrograph, and a 30 × 30 μm pixel size (Goldeye G-008 SWIR TEC1, Allied Vision Technologies GmbH, Germany). The spectral resolution was 4.6-4.7 nm (164 spectral channels per pixel from 900 nm to 1700 nm). The imaging setup incorporated an objective lens with a 25 mm focal length (F/1.4 SWIR, 0.9-1.7 μm, 21 mm image format, c-mount), positioned 220 mm above the image surface. The illumination unit consisted of four halogen lamps with Lambertian filters, mounted on an adjustable tower, which were turned on at least 20 min before image acquisition. The illumination system was powered by a Samplexpower® power converter (SEC-1223CE, Burnaby, BC, V5A 0C6, Canada), which provides a highly regulated DC output voltage of 13.8 V at 23 Amps with an AC input of 230 V at 50 Hz. Finally, a motorized linear translation stage with a range of 600 mm was also used, allowing the entire sample to be scanned while the optical systems remained fixed.

The Resonon benchtop hyperspectral imaging system was operated and processed using Spectronon PRO software. The raw reflectance readings for each sample data array were corrected by dividing the dark current-subtracted reflectance by the dark current-subtracted white standard reflectance at each corresponding wavelength (1). A dark current intensity image was collected before sample scanning to remove dark current noise by covering the camera lens. In addition, the intensity from a 99% white reflectance standard made of polytetrafluoroethylene (Spectralon™, SRT-99-120, Labsphere, North Sutton, NH, USA) was collected immediately after the dark current image to correct for illumination effects. These two images were applied to subsequent sample intensity images.

$$I = \frac{I_0 - I_b}{I_w - I_b} \quad (1)$$

where I_0 is the raw hyperspectral image obtained, I_b is the dark current reference and I_w is the white reference. Besides the dark and absolute reflectance response, the pixel illumination saturation was also adjusted with the camera controls. The framerate and the integration time were established so that no pixel in the image was saturated. Reflectance values obtained from the NIR-HSI system were stored as scaled integer reflectance (effective bit depth) as provided by the Spectronon PRO software. Consequently, reflectance values are expressed in instrument-specific digital units proportional to reflectance, although the data represent true reflectance as defined in Equation (1).

For the individual grain analysis (200 grains, 100 from each sample), each grain was scanned in three different orientations (face-up, face-down, and random). The mean spectrum was recorded for each orientation, resulting in a total of 600 spectra. After scanning, the grains were used for mycotoxin analysis.

In all the cases, a black tray was used to reduce the background noise in the image and to obtain an accurate pixel selection. Images were adjusted to 350 bands for the x-axis and approximately 90 mm for the y-axis. Pixel selection of the oat grains was done by collecting the mean reflectance values of similar spectrum pixels by Euclidian distance that is best adjusted to the region of interest to remove the background signal. Mean spectra for each grain were recorded as a text file for later exporting to the spectral analysis software.

2.4. Vis-NIR experimental work: instrumentation and data acquisition

Spectral data were collected using a LabSpec 2500® Near-Infrared Analyzer (350 to 2500 nm; Analytical Spectral Devices Inc., USA) (Fig. 1B). The instrument was equipped with three detectors: a silicon array covering 350 to 1000 nm, and two Peltier-cooled InGaAs detectors covering 1000 to 1800 nm and 1800 to 2500 nm, respectively. Measurements were taken at 1 nm intervals. Each oat grain was placed in contact with a fiber optic probe connected to an internal quartz halogen light source (Ocean Optics, USA), and spectra were recorded in digital number mode. A black bottle cap and a sample tray were used to limit the influence of external light.

Spectra were acquired for the same 200 individual oat grains, each measured three times with the grain positioned face up, face down, and

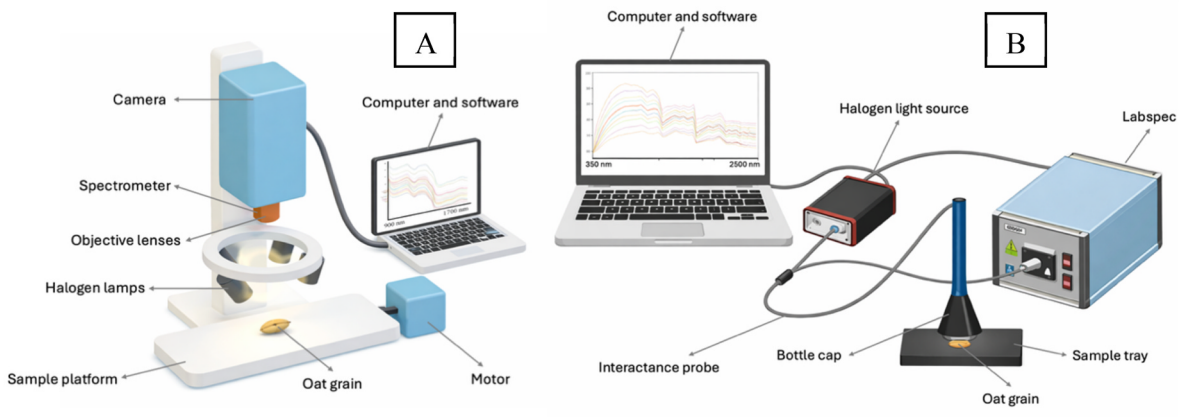


Fig. 1. Schematic representation of spectroscopic systems used for oat analysis: (A) typical visible-near infrared (Vis-NIR) spectroscopy setup, including halogen light source, interactance probe, spectrometer and data acquisition software; (B) near-infrared hyperspectral imaging (NIR-HSI) system, comprising illumination unit, camera, spectrometer, motorized translation stage and computer for hyperspectral data acquisition and processing.

at random. This procedure yielded 600 spectra, as for the NIR-HSI system (Section 2.3).

To ensure measurement stability, the analyser was powered on 50 min before starting data acquisition. Calibration was performed using a Spectralon® Diffuse Reflectance Standard before the first measurement and after every ten grains. Reflectance spectra were calculated by normalising the recorded digital numbers to the Spectralon® reference, yielding unitless reflectance values in the 0-1 range. A baseline spectrum was recorded, and three preliminary scans were conducted to verify instrument stability before collecting the complete dataset.

The LabSpec analyser was connected to an interactance probe and a light source, with spectral data acquisition managed by a computer operating Indico Pro software (Malvern Panalytical Ltd, Malvern, UK).

2.5. Determination of mycotoxin concentration in oat grains by LC-MS/MS

2.5.1. Sample preparation and mycotoxin extraction

DON, DON-3G, 15-ADON, 3-ADON, and ZEN were individually extracted from 200 oat grains, comprising 100 grains per sample. The grains were ground using a Precellys® homogenizer (Bertin Technologies, Yvelines, France). Each grain was placed into an Eppendorf tube containing a 7 mm stainless steel bead, and homogenization was performed at 5200 rpm for 2 cycles of 10 s with a 5-s interval between cycles.

After grinding, 260 μL of extraction solvent (acetonitrile, ultrapure water, and acetic acid, 79:20:1, *v/v/v*) was added to each tube. The tubes were placed on a rotary shaker (miniShaker VWR; VWR, Leighton Buzzard, UK) and agitated at 600 rpm for 90 min at 25 °C. After the extraction, the tubes were centrifuged for 5 min at 15,500×*g* (Centrifuge 5417 S, Eppendorf, Stevenage, UK) at 24 °C.

A 75 μL aliquot of the supernatant was combined with 75 μL of dilution solvent (acetonitrile, ultrapure water, and acetic acid in a 20:79:1 (*v/v/v*) ratio), and the resulting mixture was transferred into vials fitted with 250 μL microinserts.

2.5.2. LC-MS/MS procedure for mycotoxin analysis

LC-MS/MS analysis was performed using an Exion series LC system connected to a 6500+ hybrid triple quadrupole-linear ion trap mass spectrometer (qTRAP-MS) equipped with an IonDrive Turbo Spray (both Sciex Technologies, Warrington, UK). Chromatographic separation was achieved on a reversed-phase ACE-3 C^{18} column (2.1 × 100 mm, 3 μm particle size; Hichrom, Berkshire, UK) fitted with an ACE-3 guard cartridge maintained at 60 °C. The mobile phase consisted of two solvents: solvent A, composed of ultrapure water, methanol, and acetic acid (89:10:1, *v/v/v*), and solvent B, composed of ultrapure water, methanol, and acetic acid (2:97:1, *v/v/v*). Both solvents contained 5 mM ammonium acetate to facilitate ammonium adduct formation. The gradient program lasted 20 min and was set as follows: 0 min, 0% B; 2 min, 0% B; 5 min, 50% B; 14 min, 100% B; 18 min, 100% B; 19 min, 0% B. The flow rate was set to 0.6 mL/min, and the injection volume was 1 μL.

MS detection was performed in positive (ESI+) and negative (ESI-) electrospray ionisation modes, depending on the mycotoxin analysed. Source parameters were set to curtain gas at 40 psi, collision gas set at medium, ion spray voltages of −4500 V for negative and 5500 V for positive mode, temperature at 400 °C, and ion source gases 1 and 2 at 60 psi. Data were acquired in multiple reaction monitoring (MRM) mode. Retention times, precursor ions, and product ions were determined by direct infusion (syringe method) of standard reference solutions for each target compound, and these values are presented in Table 1. Optimised MS/MS parameters for individual analytes (Table 1), including collision energy, declustering potential, entrance potential, and collision cell exit potential, were established and verified using a mixed standard solution. For each mycotoxin, two or three m/z transitions were monitored. Compound identification was based on retention time and the ratio of quantifier to qualifier transitions. Data acquisition was managed using

Table 1
Method performance and MS/MS parameters for mycotoxin analysis in oat single grains using LC-MS/MS. DON = deoxynivalenol; DON-3G = deoxynivalenol-3-glucoside; 15-ADON = 15-acetyldeoxynivalenol; 3-ADON = 3-acetyldeoxynivalenol; ZEN = zearalenone; LOD = limit of detection; LOQ = limit of quantification; SD = standard deviation; RSD = relative standard deviation.

Mycotoxin	Spiking level (μg/kg)	LOD (μg/L)	LOQ (μg/L)	Recovery ± SD (%)	RSD (%)	Linearity (R^2)	Retention time (min)	Precursor ion (m/z)	Molecular ion	Product ions (m/z)[1]	Collision energy (V)	Declustering potential (V)	Entrance potential (V)	Collision cell exit potential (V)
DON	1750	5.0	16.5	100.4 ± 8.9	8.8	0.992	1.77	297.0	$[M+H]^+$	**249.1** 203.2	21	91	-	20
DON-3G	100	0.4	1.4	84.2 ± 9.1	10.8	0.992	1.93	517.1	$[M + CH_3CO_2]^-$	**457.2**417.1	−20 −30	−115	−10	−19 −11
15-ADON	75	0.4	1.2	115.3 ± 5.2	4.5	0.994	4.37	339.0	$[M+H]^+$	**260.9**320.8137.0	15 11 15	56	-	14 16 22
3-ADON	75	0.5	1.5	115.1 ± 5.8	5.1	0.990	4.33	339.0	$[M+H]^+$	**231.0**203.0 43.1	15 17 75	31	-	26 22 20
ZEN	100	0.2	0.7	115.8 ± 5.7	4.9	0.995	6.76	317.1	$[M-H]^-$	**175.01**31.2	−34 −42	−100	−10	−13 −8

[1]Quantifier ion is indicated in bold.

Analyst® software version 1.6.3, and quantification was carried out with MultiQuant™ software version 3.0.3.

2.5.3. Method validation

The analytical procedure used to quantify DON, DON-3G, 15-ADON, 3-ADON, and ZEN in individual oat grains by LC-MS/MS was validated. Method selectivity was verified by performing at least three injections of a 1 μL standard solution and comparing the resulting retention times and peak resolutions. Additional confirmation of selectivity was obtained by analysing blank, matrix, and spiked samples to identify any co-eluting peaks or interfering signals at identical *m/z* transitions. Linearity was evaluated using matrix-matched calibration curves prepared at nine concentration levels for each mycotoxin, and a determination coefficient (R^2) of 0.98 or higher was set as the acceptance threshold. Precision was determined through spiking experiments on blank oat grains over three separate days (n = 3, 3, 10), followed by calculation of recovery rates and relative standard deviations (RSDs) for each compound (Table 1). Method performance was evaluated according to the criteria established in Commission Regulation (EC) No. 2023/2782 (European Commission, 2023a). In addition, the estimation of the limits of detection (LOD) and quantification (LOQ) followed the recommendations outlined in the *Guidance Document on the Estimation of LOD and LOQ for Measurements in the Field of Contaminants in Feed and Food* (Wenzl et al., 2016) (Table 1).

2.6. Data processing for the classification of DON and ZEN contamination

Initially, spectral patterns were compared between grains that exceeded or fell below the EU regulatory limits for DON (1750 μg/kg) and ZEN (100 μg/kg). The average spectral curves for each contamination group were generated using Python version 3.12.3.

Before applying any preprocessing techniques, the spectral data were separated according to the instrument used. For the NIR-HSI system (900-1700 nm), 600 spectra were obtained from 200 grains scanned three times each. An equivalent number of spectra were recorded for the Vis-NIR system (350-2500 nm). To minimise edge scattering and instrument noise, the spectral range was restricted to 1000-1600 nm for NIR-HSI and 380-2470 nm for Vis-NIR.

Several preprocessing strategies were evaluated to determine their influence on classification performance. The raw spectra were retained as a baseline, while the standard normal variate (SNV) transformation was applied to correct for multiplicative scattering and standardise intensity values among samples. The 1st derivative of the spectra was also calculated to emphasise minor absorption features and to eliminate baseline shifts. Based on these techniques, five datasets were constructed: raw data, SNV, 1st derivative, SNV followed by 1st derivative, and 1st derivative followed by SNV. Each combination was analysed to identify the most effective preprocessing method for enhancing discrimination of DON- and ZEN-contaminated grains.

Exploratory principal component analysis (PCA) of single-grain spectra was not repeated in the present study, as the influence of sample origin, grain orientation and contamination level on spectral structure had been previously evaluated using near-infrared hyperspectral imaging at the individual-grain level (Teixido-Orries, Molino, Femenias, et al., 2023). That analysis showed no dominant clustering attributable to origin or grain orientation and indicated that unsupervised PCA was insufficient to reliably discriminate contaminated grains, thereby supporting the use of supervised classification approaches in the present work.

Toxin concentration values were converted into binary classes prior to classification. Grains with DON or ZEN levels above the EU legal limits (1750 μg/kg and 100 μg/kg, respectively) were labelled as contaminated (1), while those below the limits were labelled as non-contaminated (0). A soft-voting ensemble classifier was developed by combining logistic regression and partial least squares (PLS) regression models. Logistic regression was selected for its robustness and interpretability under class imbalance, while PLS regression was included to capture latent spectral structures commonly exploited in chemometric analysis. The logistic regression component was configured with balanced class weights to address class imbalance, using the liblinear solver. The PLS regression component was parameterised with the number of latent variables calculated as the minimum between the square root of training samples and one-tenth of the feature count. Both models were preceded by StandardScaler normalisation within their respective pipelines. PLS regression outputs were linearly rescaled to the [0,1] range using min–max scaling on training data, enabling probability-like interpretation within the ensemble.

Final ensemble predictions were computed as a weighted combination of probability outputs from logistic regression and probability-like scores derived from PLS regression. Optimal weights for each component model were determined through grid search, evaluating weight combinations from 0.0 to 1.0 in increments of 0.05, where the PLS weight was constrained as the complement of the logistic regression weight. The classification threshold was simultaneously optimised by evaluating 50 threshold values ranging from 0.05 to 0.95.

Model performance was validated using stratified 10-fold cross-validation to preserve class proportions across folds. Within each training fold, ensemble weights and decision thresholds were optimised exclusively on the training data to maximise the F1-score for the contaminated class (positive), ensuring strict separation between training and testing partitions. Classification accuracy (CA) and F1-score for the positive class were computed for each fold, and overall performance was determined by averaging results across all folds along with standard deviations (SDs). Three classification thresholds were examined: (i) DON contamination, (ii) ZEN contamination, and (iii) grains contaminated with either DON or ZEN. The three thresholds were combined with the five preprocessing approaches, generating a total of 15 classification configurations for each spectroscopic technique.

Permutation importance was computed within each cross-validation fold by randomly shuffling individual spectral variables 30 times and quantifying the resulting decrease in F1-score. Feature importance values were averaged across folds to obtain robust estimates and associated SDs. The 20 most influential spectral features were extracted. To evaluate the potential for dimensionality reduction, the ensemble models were retrained using only the top 20 most important features as identified by permutation importance analysis. The same cross-validation procedure was applied to these reduced-feature models, and their performance was compared against the full-feature baseline. To further assess the feasibility of more compact multispectral configurations for real-time applications, additional reduced-feature models were also evaluated using the top 10 and top 5 wavelengths. Models based on 20, 10 and 5 wavelengths were trained and evaluated using identical preprocessing, classification, and validation procedures, allowing a direct comparison of predictive performance and computational efficiency across different levels of spectral dimensionality.

The most accurate classifiers were selected based on F1-score and CA. Confusion matrices were produced for all models by aggregating predictions across all cross-validation folds, providing an overall assessment of classification performance. Receiver operating characteristic (ROC) curves were plotted, from which the area under the curve (AUC) values were calculated to assess classification reliability. Higher F1-score, CA, recall (true positive rate), and specificity (true negative rate) indicated stronger predictive performance, while AUC values approaching 1.0 denoted excellent discriminative ability and values close to 0.5 reflected random classification.

Prediction time was measured for each model configuration to assess computational efficiency. Throughput was calculated as samples processed per second, enabling comparison between full-feature and reduced-feature models.

All analyses were performed using Python version 3.12.3, employing Scikit-Learn 1.3.2 for classification tasks and cross-validation, and additional libraries such as NumPy 1.26.4 and Pandas 2.2.3 for data

manipulation and computation.

3. Results and discussion

3.1. Comparison of spectral profiles of oat grains with different DON and ZEN levels

Fig. 2 presents the average spectral reflectance profiles of individual oat grains classified according to their contamination levels of DON and zearalenone ZEN, based on EU legal thresholds (1750 μg/kg for DON and 100 μg/kg for ZEN). Reflectance spectra were obtained using both NIR-HSI (1000-1600 nm) and Vis-NIR (380-2470 nm) systems and are shown separately for DON (Fig. 2A and B) and ZEN (Fig. 2C and D).

In the case of DON, spectral differences between more and less-contaminated grains are subtle but noticeable. In the NIR-HSI spectra (Fig. 2A), grains with lower DON levels show slightly less reflectance between 1000 and 1200 nm. The curves then converge, and beyond 1400 nm, grains with lower DON levels tend to exhibit greater reflectance. In the Vis-NIR spectra (Fig. 2B), there is general overlap throughout most of the spectra, though some distinction appears in the 800-1400 nm and 1600-1900 nm regions, where less-contaminated grains tend to have slightly lower reflectance.

For ZEN, a similar trend is observed. In the NIR-HSI spectra (Fig. 2C), grains with high ZEN levels initially present increased reflectance, followed by convergence, and later slightly lower reflectance beyond 1400 nm. In the Vis-NIR spectra (Fig. 2D), substantial overlap is present overall. However, in 380-800 nm range, grains with elevated ZEN levels exhibit lower reflectance, suggesting subtle changes in surface coloration. Additionally, between 900 and 1400 nm, more-contaminated grains tend to show stronger reflectance, whereas in the 1900-2500 nm region, grains with lower ZEN content exhibit increased reflectance.

These findings align with previous research on spectral variability associated with mycotoxin contamination in cereals. In previous studies, some overlap was observed in the NIR region (900-1700 nm) between oat samples contaminated with DON and T-2 and HT-2 toxins at levels above and below their EU legal limits, like the overlapping trends observed in a study at the established thresholds (Teixido-Orries et al., 2026; Teixido-Orries, Molino, Femenias, et al., 2023; Teixido-Orries, Molino, Gatius, et al., 2023). The extensive spectral overlap observed between contamination groups is inherent to Vis-NIR spectroscopy, where absorption features arise from broad overtone and combination bands shared by the cereal matrix and fungal-related compounds. As discussed in Section 3.4, discrimination therefore relies on subtle, multivariate spectral patterns rather than on distinct marker bands. Tekle et al. (2013) also investigated the use of Vis-NIR spectroscopy for estimating DON levels in ground oat samples. Their study showed that the spectral signatures of samples with low and high DON concentrations were largely comparable; however, highly contaminated samples exhibited greater absorption in the Vis range and lower absorption in the NIR range. In agreement with those findings, our data revealed that increased contamination was generally associated with higher reflectance within the NIR region (900-1400 nm) and reduced reflectance in the Vis region (380-800 nm).

Altogether, these results demonstrate that although the spectral differences between groups are not large, they normally occur in chemically relevant regions. The most consistent separation occurs in the NIR range, particularly between 900 and 1400 nm, likely corresponding to absorption bands of water, protein, and starch. This suggests that this region may be associated with chemical and physical changes in oat grains due to fungal infection and mycotoxin production. However, these subtle shifts support the feasibility of using chemometric approaches to distinguish contaminated from uncontaminated grains and justify further development of classification models.

3.2. Grain weight distribution and relationship with mycotoxin contamination

The weights of the 200 individual grains ranged from 20.1 to 56.8 mg, with a mean value of 41.9 mg, a median of 43.1 mg, and a SD of 6.7 mg, corresponding to a coefficient of variation of 15.9%. This level of variability reflects the natural heterogeneity typically observed within oat batches.

Correlation analysis between grain weight and mycotoxin concentration revealed a weak negative relationship across all compounds analysed. Pearson correlation coefficients were −0.106 for DON, −0.113 for DON-3G, −0.079 for 15-ADON, −0.077 for 3-ADON, and

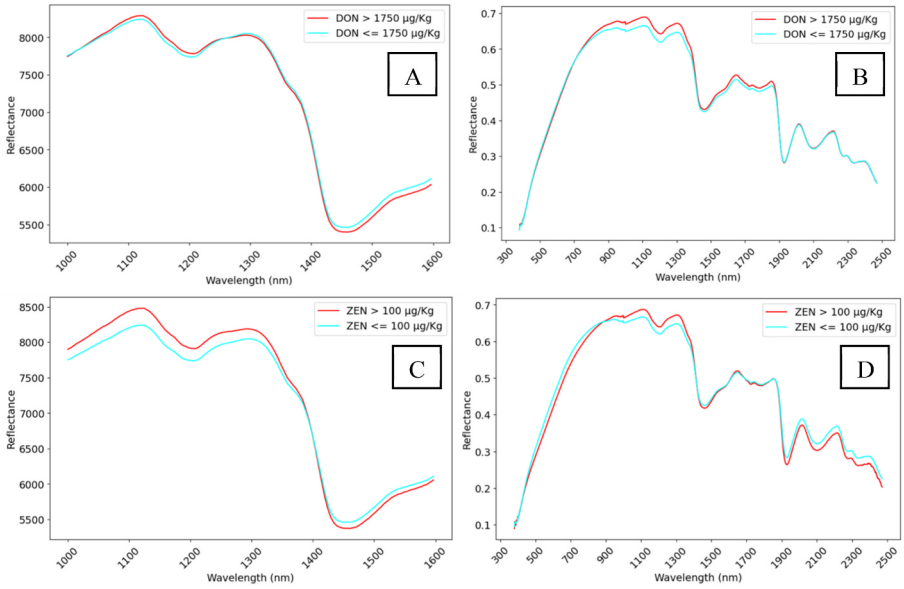


Fig. 2. Mean spectral reflectance profiles of oat grains classified by their contamination levels of deoxynivalenol (DON) and zearalenone (ZEN), relative to the legal limits (1750 μg/kg for DON and 100 μg/kg for ZEN). (A–B) Spectral profiles for DON-contaminated grains above and below the legal limit using (A) near-infrared hyperspectral imaging (NIR-HSI) and (B) visible-near infrared (Vis-NIR) spectroscopy. (C–D) Spectral profiles for ZEN-contaminated grains above and below the legal limit using (C) NIR-HSI and (D) Vis-NIR spectroscopy. All panels show reflectance data; differences in y-axis scale arise from instrument-specific reflectance scaling, with NIR-HSI spectra expressed as reflectance values scaled to the effective bit depth of the camera and Vis-NIR spectra expressed as normalized reflectance (0–1).

−0.136 for ZEN. Although these correlations were low and indicate that grain weight is not a strong predictor of mycotoxin concentration, they suggest a general tendency for higher contamination levels to be associated with lighter grains.

To further explore this relationship, grains were classified according to contamination status (>LOD vs. <LOD). No statistically significant differences in grain weight were observed between contaminated and uncontaminated grains for any of the mycotoxins analysed ($p > 0.05$). Nevertheless, a consistent trend was observed across these five mycotoxins, whereby contaminated grains exhibited slightly lower mean weights than uncontaminated grains, corresponding to an average reduction of 3.9%. This observation is consistent with the negative correlations observed between grain weight and mycotoxin concentration.

Comparable trends have been reported in previous studies on oats affected by *Fusarium species*. Modest reductions in grain weight associated with fungal infection have been described, although the relationship between grain mass and mycotoxin content is generally weak (Martinelli et al., 2014). Other studies have reported that high DON contamination is more strongly related to compositional traits, such as protein content or hull-to-groat ratio, rather than to grain weight alone (Yan et al., 2017). Likewise, infection by *F. langsethiae* has been shown to alter grain composition without producing significant changes in grain mass (Martin et al., 2018).

3.3. Potential effect of grain-level sorting on mycotoxin reduction in oat batches

The individual mycotoxin content of 200 oat grains was analysed by LC-MS/MS. As shown in Fig. 3, the concentration of DON, its modified forms (DON-3G, 15-ADON, and 3-ADON), and ZEN varied widely across the sample set. While most grains contained low or undetectable levels, a small proportion exhibited extremely high concentrations of one or more mycotoxins. To further illustrate this heterogeneity and the resulting class imbalance, the distributions of single-grain mycotoxin concentrations are shown as histograms in Figs. S1 and S2, highlighting the strongly skewed nature of the data and the small proportion of grains exceeding the EU regulatory limits.

The mean concentration of each mycotoxin across the full sample set was first calculated. To calculate the overall average for each mycotoxin, a LOD/$\sqrt{2}$ value was used for grains with values below the LOD. DON showed a particularly high average value of 4507 μg/kg, while the mean concentrations of DON-3G, 15-ADON, and 3-ADON were 1721 μg/kg, 116 μg/kg, and 340 μg/kg, respectively. The average ZEN concentration was 9.0 μg/kg. Analysis of individual grains revealed that 8% exceeded the legal threshold for DON, 2% exceeded the limit for ZEN, and 9% exceeded at least one of the two limits. These data confirm the heterogeneous nature of mycotoxin contamination in oat batches and the potential value of grain-level classification and removal strategies.

To evaluate the effectiveness of such an approach, three removal simulations were performed, each based on eliminating grains that exceeded specific regulatory thresholds. When only grains with DON concentrations above 1750 μg/kg were removed, the average DON concentration across the remaining batch was reduced by 89.3%, from 4507 to 482 μg/kg. This intervention also markedly reduced the concentrations of DON-3G (−98.0%), 15-ADON (−95.2%), and 3-ADON (−95.5%). Although ZEN was not directly targeted, its concentration also decreased by 54.0%, likely due to partial co-contamination with DON.

In contrast, removing only grains exceeding the legal limit for ZEN (100 μg/kg) yielded more modest improvements. The average ZEN concentration declined by 45.5%, from 9.0 to 4.9 μg/kg. However, this reduction appears less pronounced than for other mycotoxins, partly because initial ZEN levels were already low and values below the LOD were replaced by LOD/$\sqrt{2}$, which limits the observable decrease. By comparison, the concentrations of DON and its derivatives showed clearer reductions, with DON decreasing by 57.8%. The reductions in DON-3G, 15-ADON, and 3-ADON ranged from 53.1% to 61.2%, suggesting that in some cases, ZEN-contaminated grains also contain other mycotoxins.

A third simulation involved removing all grains that exceeded either 1750 μg/kg for DON or 100 μg/kg for ZEN. This combined strategy further reduced the mean DON concentration to 472 μg/kg (−89.5%) and was equally effective as the DON-only strategy in lowering DON derivatives, with decreases of −98.1% for DON-3G, −95.2% for 15-ADON, and −95.7% for 3-ADON. Interestingly, ZEN levels declined more strongly under the combined strategy (3 μg/kg, −67.0%) than when applying the ZEN-only criterion, likely because some grains above the DON threshold were also co-contaminated with ZEN. These results show that the simultaneous application of DON and ZEN thresholds provides the same benefits as DON-targeted sorting for DON and its derivatives, while achieving stronger reductions in ZEN, thereby broadening the safety benefits in co-contaminated batches.

Overall, these findings confirm that a small number of highly contaminated grains are responsible for most of the mycotoxin burden in oat batches. Targeted grain removal based on non-destructive screening could therefore lead to substantial reductions in overall contamination, even when only a minority of grains are discarded. Moreover, the strong correlation between DON and its modified forms suggests that detection of DON alone may be sufficient to achieve broad-spectrum mycotoxin mitigation in many cases. Therefore, these results provide a clear rationale for developing methods to detect individual grains that exceed regulatory thresholds. As such, the subsequent sections of this study investigate the potential of Vis-NIR spectroscopy and NIR-HSI as rapid, non-destructive tools for identifying highly contaminated grains based on their spectral characteristics.

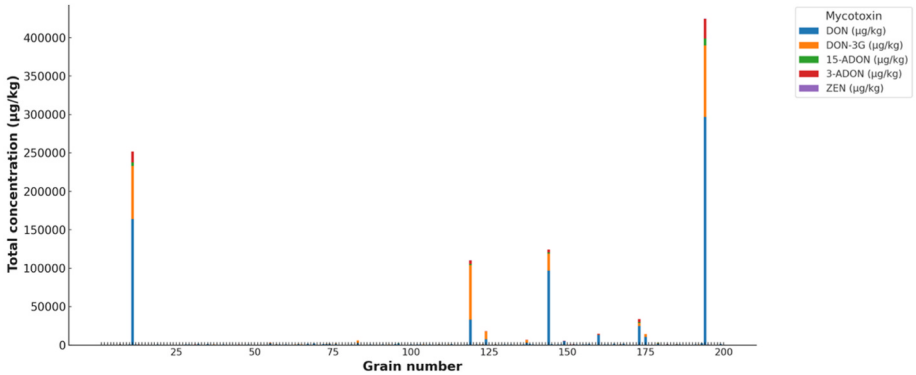


Fig. 3. Concentrations of deoxynivalenol (DON), DON-3-glucoside (DON-3G), 15-acetyldeoxynivalenol (15-ADON), 3-acetyldeoxynivalenol (3-ADON), and zearalenone (ZEN) in 200 individual oat grains. Each bar represents one grain, and colours indicate the relative concentration of each mycotoxin.

3.4. Classification of individual oat grains according to the EU legal limit for DON (1750 μg/kg)

Table 2 presents the results of the 10 classification models for discriminating individual unprocessed oat grains from those exceeding the EU legal limit (1750 μg/kg) for DON, using NIR-HSI and Vis-NIR spectroscopy with various pre-processing techniques. F-1 score, CA and AUC varied depending on the pre-processing and the spectroscopic technique applied.

For NIR-HSI, the two best-performing models were obtained using SNV followed by 1st derivative preprocessing and 1st derivative followed by SNV. These models achieved CAs of 94 ± 4 % and 92 ± 8 %, respectively, together with the highest and most stable F1-scores for the contaminated class (0.68 ± 0.12 and 0.68 ± 0.14). The corresponding AUC values (0.89-0.90) indicate strong global discriminative ability, confirming that NIR-HSI provides reliable separation between grains above and below the regulatory threshold.

In contrast, Vis-NIR spectroscopy showed lower performance for DON classification, particularly for the contaminated (minority) class. The best Vis-NIR models (raw spectra and SNV preprocessing) achieved CAs of 91 ± 5 % and 87 ± 11 %, with AUC values ranging from 0.60 to 0.75, indicating only moderate separability. Despite acceptable CA values, the low F1-scores (0.44-0.48) reveal limited sensitivity towards highly contaminated grains, reflecting difficulties in reliably identifying extreme contamination events.

The superior performance of NIR-HSI compared with Vis-NIR can be attributed to fundamental differences in data acquisition. NIR-HSI captures spectral information from hundreds of pixels per grain, enabling spatial averaging and integration of heterogeneous spectral features across the entire grain surface. This approach provides a more representative description of grain condition, particularly for contamination that may be unevenly distributed. In contrast, Vis-NIR measurements rely on a single-point contact spectrum, which samples only a limited portion of the grain and is therefore more sensitive to local variability, grain orientation and surface contact effects.

To our knowledge, this is the first study to classify naturally contaminated individual oat grains by DON content using spectroscopic techniques. In previous research, 8 g samples of naturally contaminated oat were classified based on their DON and T-2 and HT-2 content toxins, achieving maximum CAs of 83% and 94%, respectively (Teixido-Orries, Molino, Femenias, et al., 2023; Teixido-Orries, Molino, Gatius, et al., 2023), which were comparable to the results obtained in the present study. According to the existing literature, the only reported attempt to build classification models for single oat grains in relation to DON content was that of Tekle et al. (2015). In that work, NIR-HSI was employed to analyse individual pixels of oat grains that had been artificially inoculated with *Fusarium* spores. The proportion of pixels exhibiting visible damage was used as a metric to differentiate among visual categories of infection and associated DON concentrations. Their study demonstrated that NIR-HSI could identify grains with elevated DON even when no clear external symptoms were visible. However, the experiments relied exclusively on artificially contaminated material.

Table 2
Classification accuracies (CAs), F-1 score, confusion matrix, area under the curve (AUC) and most characteristic wavelengths for validation sets in the classification models of oat grains according to the European Union (EU) legal limit of deoxynivalenol (DON) (1750 μg/kg), obtained using a soft-voting ensemble classifier (logistic regression + partial least squares (PLS) regression). U = grains above the legal limit; L = grains below the legal limit; SD = standard deviation.

Equipment	Pre-treatment	Confusion matrix (%)				CA (%) ± SD	AUC	F1-score ± SD	Most characteristic wavelength (nm)
NIR-HSI (1000-1600 nm)	Raw data	Actual	Predicted			92 ± 5	0.90	0.64 ± 0.14	1353
				U	L				
			U	75	25				
			L	6	94				
	SNV	Actual	Predicted			94 ± 2	0.89	0.67 ± 0.09	1481
				U	L				
			U	73	27				
			L	4	96				
	1st derivative	Actual	Predicted			94 ± 3	0.88	0.65 ± 0.14	1486
				U	L				
			U	65	35				
			L	3	97				
	1st derivative + SNV	Actual	Predicted			92 ± 8	0.89	0.68 ± 0.14	1491
				U	L				
			U	79	21				
			L	7	93				
	SNV + 1st derivative	Actual	Predicted			94 ± 4	0.90	0.68 ± 0.12	1312
				U	L				
			U	77	23				
			L	5	95				
Vis-NIR (380-2470 nm)	Raw data	Actual	Predicted			91 ± 5	0.73	0.44 ± 0.15	2336
				U	L				
			U	40	60				
			L	4	96				
	SNV	Actual	Predicted			87 ± 11	0.75	0.48 ± 0.18	417
				U	L				
			U	60	40				
			L	11	89				
	1st derivative	Actual	Predicted			88 ± 6	0.60	0.35 ± 0.12	846
				U	L				
			U	42	58				
			L	8	92				
	1st derivative + SNV	Actual	Predicted			87 ± 10	0.64	0.40 ± 0.17	846
				U	L				
			U	46	54				
			L	9	91				
	SNV + 1st derivative	Actual	Predicted			88 ± 9	0.65	0.42 ± 0.16	700
				U	L				
			U	48	52				
			L	9	91				

Subsequently, Teixido-Orries, Yang, et al. (2025) implemented Vis-NIR spectroscopy to classify artificially contaminated oat grains according to the presence of other trichothecenes, specifically T-2 and HT-2 toxins, achieving a CA of 93%. In a later investigation, Teixido-Orries et al. (2026) applied both Vis-NIR and HSI-NIR spectroscopy to distinguish naturally contaminated oats with respect to the regulatory thresholds for T-2 and HT-2, reporting maximum CA of 90% and 93%, respectively. Similar strategies have also been adopted for other cereals. Barbedo et al. (2017) developed classification models for DON detection in single wheat kernels, with a reported accuracy of 84%. Femenias et al. (2021) later discriminated individual wheat grains according to the legal limit for DON with a CA of 99%, while in the following investigation, the same authors achieved a maximum of 86% (Femenias et al., 2022).

DON concentration in oats is relatively low compared to the major constituents of the grain, such as starch, protein, fibre, and water. As a result, DON cannot be directly detected by Vis-NIR spectroscopy or NIR-HSI, since the toxin itself does not produce distinct spectral features. Instead, classification models rely on detecting the indirect effects of *Fusarium* infection, such as changes in the chemical composition and physical characteristics of the grain that result from fungal growth and mycotoxin synthesis. These changes can be captured by spectral differences across the Vis and NIR regions, even though they are driven by different mechanisms. The Vis region is especially useful for identifying surface-level physical characteristics such as discoloration, morphological defects, and surface damage. In contrast, the NIR region is more sensitive to internal chemical and structural features, including protein and moisture content, starch, and fibre composition (Walsh et al., 2020). This dual functionality explains the utility of both spectral regions in mycotoxin detection in cereals, with each capturing complementary information about grain condition.

In this study, several of the most relevant wavelengths for classifying DON contamination were found in the NIR region, notably between 1000 and 1250 nm and between 1300 and 1500 nm (Table 5). Earlier studies also identified NIR wavelengths relevant to DON detection in oat samples, including 1149, 1154, 1198, 1203, 1208, and 1388 nm (Teixido-Orries, Molino, Femenias, et al., 2023). Many of these wavelengths overlap with those identified as most influential in the present study, such as 1052, 1097, 1198, 1252, 1312, 1343, 1383, 1404, 1409, 1429, 1481, and 1491 nm. The complex NIR spectra of oat grains arise from multiple overtone and combination bands of organic bonds, particularly C-H (aliphatic and aromatic), C-O, O-H, and N-H (amide and amine) bonds (Meenu et al., 2022). In particular, the 1000-1250 nm range is associated with C-H and N-H combination bands, typically linked to carbohydrate and protein structures, respectively. Moreover, bands around 1400 nm correspond primarily to the first overtone of O-H stretching, as well as combinations involving C-H bonds, and are therefore associated with carbohydrates, organic molecules, and water content (Badr Eldin, 2010). Notably, NIR has also been shown to discriminate between oat and groat (oat without hull) based on wavelengths such as 1132, 1195 and 1608 nm (Redaelli & Berardo, 2002; Serranti et al., 2013), highlighting the sensitivity of this spectral region to hull-related structural differences. Moreover, β-glucan-related spectral bands have been observed around 1200, 1450, 1750, 1950, 2100, 2300, and 2500 nm in oats (Meenu et al., 2022). Consistently, 1200 nm and 1450 nm, previously linked to β-glucans, were also identified as informative in this study, together with bands in the 2300-2500 nm range for Vis-NIR models. Moreover, Tekle et al. (2013) analysed DON contamination in ground oat samples using Vis-NIR spectroscopy and reported a prominent band at 1432 nm, which they associated with water content, indicating that samples with higher DON levels tended to exhibit lower moisture. This observation is consistent with our results, in which wavelengths around 1400 nm repeatedly emerged as relevant, supporting the role of O-H overtone absorptions and moisture-related changes as indirect spectral markers of DON contamination. In a previous work, Yan et al. (2017) reported that oat cultivars highly contaminated with DON tended to have higher protein content and a greater hull-to-groat ratio. Similarly, Martin et al. (2018) indicated that infection by *Fusarium langsethiae*, a key producer of type A trichothecenes, resulted in alterations to β-glucan levels in oats. Furthermore, previous research has attributed wavelengths around 1200 nm and 1400 nm to *Fusarium*-induced damage in cereals (Delwiche et al., 2019; Tekle et al., 2013). Taken together, these findings suggest that the NIR-based discrimination of DON-contaminated oat grains primarily reflects indirect biochemical and structural changes, particularly involving protein composition, hull structure, moisture distribution, and fibre content.

In the visible region, wavelengths between 400 and 465 nm emerged as influential features in the Vis-NIR classification models (Table 5). This finding is supported by previous studies: Tekle et al. (2013) identified wavelengths around 492 nm as key for differentiating between low- and high-DON oat samples, while Teixido-Orries, Yang, et al. (2025) and Teixido-Orries et al. (2026) highlighted the 430-630 nm region as the most relevant for classifying oat grains contaminated with T-2 and HT-2 toxins (trichothecenes type A). Although this study focused on naturally contaminated samples, artificial contamination has been associated with visual changes in grain appearance. For instance, Tekle et al. (2013) noted that oats artificially inoculated with DON-producing *Fusarium* strains exhibited slight but detectable darkening. Such discolouration, commonly associated with brownish hues in infected hulls and caryopses, may not always be perceptible to the human eye but can be detected in the Vis spectra and leveraged for classification.

In summary, the ability of Vis-NIR and NIR-HSI techniques to identify DON-contaminated oat grains stems from their capacity to detect indirect spectral traits related to *Fusarium*-induced changes in protein, fibre, β-glucans, hull, and coloration characteristics.

3.5. Classification of individual oat grains according to the EU legal limit for ZEN (100 μg/kg)

Table 3 presents the 10 classification models for discriminating individual oat grains based on the EU legal limit for ZEN (100 μg/kg), using NIR-HSI and Vis-NIR spectroscopy combined with various spectral pre-processing techniques. As observed in the DON classification (Section 3.4), pre-processing of spectral data and spectroscopic technique had a substantial impact on classification performance.

For NIR-HSI, classification results were consistently excellent across all configurations. The two best-performing models were obtained using SNV and 1st derivative plus SNV pre-processing, both achieving CAs of 99 ± 1%, F1-scores between 0.89 ± 0.14 and 0.90 ± 0.16, and AUC values of 0.97, indicating outstanding discriminative ability and high robustness. Raw spectra also performed well (CA = 98 ± 2%, AUC = 0.97), although with a lower F1-score (0.73 ± 0.24), reflecting reduced sensitivity for the contaminated class.

For Vis-NIR spectroscopy, the best results were achieved using raw spectra and SNV pre-processing. These models reached CAs of approximately 93%, F1-scores between 0.68 ± 0.32 and 0.70 ± 0.36, and AUC values of 0.89-0.91, indicating good but clearly lower discriminative performance compared with NIR-HSI. In contrast, derivative-based preprocessing strategies led to a marked deterioration in performance, with reduced F1-scores and increased variability, suggesting that Vis-NIR spectra are more sensitive to noise amplification when derivatives are applied. This behaviour mirrors that observed for DON classification and reinforces the importance of selecting preprocessing strategies tailored to each technique. Moreover, consistent with the DON results, NIR-HSI clearly outperformed Vis-NIR in terms of classification robustness, F1-score, and AUC.

To the best of our knowledge, this is the first study to classify individual oat grains according to ZEN content using spectroscopic methods. The only previous study addressing ZEN detection via NIR was that of Ning et al. (2022), who applied NIR spectroscopy to quantify ZEN levels in wheat kernels using regression models. Their best model achieved high predictive accuracy (correlation coefficient of 0.99) and a low

Table 3
Classification accuracies (CAs), F-1 score, confusion matrix, area under the curve (AUC) and most characteristic wavelengths for validation sets in the classification models of oat grains according to the European Union (EU) legal limit of zearalenone (ZEN) (100 μg/kg). Obtained using a soft-voting ensemble classifier (logistic regression + partial least squares (PLS) regression). U = grains above the legal limit; L = grains below the legal limit; SD = standard deviation.

Equipment	Pre-treatment	Confusion matrix (%)				CA (%) ± SD	AUC	F1-score ± SD	Most characteristic wavelength (nm)
NIR-HSI (1000-1600 nm)	Raw data	Actual	Predicted			98 ± 2	0.97	0.73 ± 0.24	1096
				U	L				
			U	100	0				
			L	3	97				
	SNV	Actual	Predicted			99 ± 1	0.97	0.89 ± 0.14	1193
				U	L				
			U	100	0				
			L	1	99				
	1st derivative	Actual	Predicted			99 ± 2	0.95	0.83 ± 0.21	1277
				U	L				
			U	92	8				
			L	1	99				
	1st derivative + SNV	Actual	Predicted			99 ± 1	0.97	0.90 ± 0.16	1277
				U	L				
			U	100	0				
			L	1	99				
	SNV + 1st derivative	Actual	Predicted			99 ± 2	0.96	0.88 ± 0.18	1277
				U	L				
			U	100	0				
			L	1	99				
Vis-NIR (380-2470 nm)	Raw data	Actual	Predicted			93 ± 13	0.89	0.70 ± 0.36	2360
				U	L				
			U	100	0				
			L	7	93				
	SNV	Actual	Predicted			93 ± 16	0.91	0.68 ± 0.32	1121
				U	L				
			U	100	0				
			L	7	93				
	1st derivative	Actual	Predicted			86 ± 14	0.74	0.34 ± 0.35	1678
				U	L				
			U	67	33				
			L	13	87				
	1st derivative + SNV	Actual	Predicted			84 ± 17	0.70	0.34 ± 0.35	1678
				U	L				
			U	75	25				
			L	16	84				
	SNV + 1st derivative	Actual	Predicted			81 ± 18	0.73	0.36 ± 0.35	1673
				U	L				
			U	83	17				
			L	19	81				

root-mean-square error of prediction (2.1 μg/kg), demonstrating the feasibility of high-precision ZEN prediction in cereals. However, their study focused on quantification, not classification; on wheat, not oats; and on ground, not intact grains. Additionally, their thresholds were not aligned with regulatory limits, further highlighting the novelty of our approach.

As discussed in Section 3.4 for DON, the detection of ZEN via Vis-NIR and NIR-HSI is unlikely to arise from direct spectral absorption by the toxin itself, given its low concentration relative to bulk grain constituents. Rather, the discrimination achieved is most probably due to secondary effects of fungal colonisation. ZEN frequently co-occurs with DON and its modified forms in naturally contaminated grains, with observed correlations of approximately 0.5 (Fredlund et al., 2013; Teixido-Orries, Molino, et al., 2025). This co-occurrence arises because both toxin groups are primarily produced by the same *Fusarium species* (*F. graminearum* and *F. culmorum*), although typically under different environmental conditions. While the specific metabolic effects of ZEN contamination on oat grain composition are not well characterised, it is plausible to hypothesise similar outcomes to those reported for DON, including changes in hull structure, protein, moisture, and β-glucan content. These biological associations further justify the high CA achieved in this study and suggest that spectral methods targeting structural and compositional alterations may be effective for the simultaneous detection of multiple mycotoxins. Compared with DON, ZEN classification yielded consistently higher accuracies, F1-scores and AUC values across both spectroscopic techniques. These results suggest that ZEN contamination may be associated with more pronounced and/or more spatially coherent biochemical and physical alterations within oat grains compared with DON. It is plausible that the infection patterns and metabolic processes associated with ZEN production induce more consistent structural or compositional changes, which are particularly well captured by NIR-HSI due to its spatially resolved acquisition and averaging across the entire grain surface.

The analysis of the most relevant wavelengths selected for ZEN classification revealed strong similarities with those identified for DON contamination (Table 5). For NIR-HSI models, most influential wavelengths were concentrated in the NIR regions between 1000-1200 nm and 1300-1500 nm. These spectral intervals coincide with those previously associated with *Fusarium*-related alterations in oat grains and were also dominant in the DON classification models. Similarly, Vis-NIR models for ZEN showed relevant wavelengths in the Vis region (approximately 380-460 nm) and in the longer-wavelength NIR region around 2300-2500 nm, mirroring the spectral patterns observed for DON. As discussed in Section 3.4, these regions are linked to indirect effects of fungal infection, such as changes in grain surface colour, hull structure, protein composition, moisture distribution and fibre-related components. The strong overlap between the spectral regions selected for DON and ZEN classification supports the hypothesis that both toxins induce comparable biochemical and structural modifications in oat grains. Importantly, several of the most relevant wavelengths reported by Ning et al. (2022), primarily between 950 and 1550 nm, overlap with those identified in our study. Their wavelength selection algorithms

repeatedly emphasised bands around 1000-1250 nm and 1400-1550 nm. This overlap with our findings strengthens the evidence that these regions contain indirect spectral signatures associated with ZEN contamination and its underlying effects on grain composition.

3.6. Classification of individual oat grains exceeding the EU legal thresholds for both DON and ZEN

Considering the frequent co-occurrence of DON, its modified forms, and ZEN in oat grains, a combined classification model capable of detecting samples exceeding both EU regulatory thresholds offers a practical and efficient solution. This approach allows the identification of grains contaminated with either toxin using a single model, which is advantageous for implementation in industrial screening systems. Table 4 summarises the performance of the classification models developed to identify oat grains exceeding both legal limits (1750 μg/kg for DON and 100 μg/kg for ZEN), using NIR-HSI and Vis-NIR spectroscopy.

For NIR-HSI, the best-performing models were obtained using SNV and SNV combined with 1st derivative pre-processing. These models achieved CAs of 93 ± 4% and 93 ± 3%, respectively, with F1-scores between 0.64 ± 0.13 and 0.66 ± 0.13, and AUC values close to 0.89, indicating good discriminative ability and robust identification of grains exceeding at least one regulatory threshold.

For Vis-NIR spectroscopy, the best results were obtained using raw spectra and SNV pre-processing, yielding CAs of 91 ± 5% and 92 ± 4%, respectively, with F1-scores of 0.47 ± 0.10 and 0.51 ± 0.12. Although these results demonstrate the feasibility of Vis-NIR for combined DON + ZEN screening, performance was consistently lower than that achieved with NIR-HSI.

Overall, NIR-HSI outperformed Vis-NIR for combined DON + ZEN classification, in agreement with the trends observed for the individual DON and ZEN models. Importantly, the classification performance obtained for the combined DON + ZEN models closely mirrors that observed for DON alone (Section 3.4). Consequently, the inclusion of ZEN in the combined model does not compromise classification performance but rather extends the practical applicability of the approach by enabling simultaneous screening for multiple mycotoxins within a single classification framework.

Analysis of the most relevant wavelengths selected for the combined DON + ZEN models shows that they largely fall within the same spectral regions identified for the individual DON and ZEN classifications, particularly in the Vis range around 400-460 nm, the NIR region between 1000-1250 nm and 1300-1500 nm, and, for Vis-NIR models, the longer-wavelength region around 2300-2400 nm (Table 5). These spectral intervals have already been associated with *Fusarium*-related alterations in grain composition and structure, as discussed in previous sections. Although some individual wavelengths selected in the combined DON + ZEN models did not appear among the top-ranked features of the individual DON or ZEN models, they remained within these same

Table 4
Classification accuracies (CAs), F-1 score, confusion matrix, area under the curve (AUC) and most characteristic wavelengths for validation sets in the classification models of oat grains according to the European Union (EU) legal limit of deoxynivalenol (DON) (1750 μg/kg) and zearalenone (ZEN) (100 μg/kg), obtained using a soft-voting ensemble classifier (logistic regression + partial least squares (PLS) regression). U = grains above the legal limits; L = grains below the legal limits; SD = standard deviation.

Equipment	Pre-treatment	Confusion matrix (%)				CA (%) ± SD	AUC	F1-score ± SD	Most characteristic wavelength (nm)
NIR-HSI (1000-1600 nm)	Raw data	Actual	Predicted			92 ± 6	0.88	0.65 ± 0.15	1497
				U	L				
			U	72	8				
			L	6	94				
	SNV	Actual	Predicted			93 ± 4	0.88	0.66 ± 0.13	1481
				U	L				
			U	72	8				
			L	5	95				
	1st derivative	Actual	Predicted			91 ± 7	0.88	0.63 ± 0.14	1486
				U	L				
			U	76	24				
			L	8	92				
	1st derivative + SNV	Actual	Predicted			93 ± 3	0.89	0.64 ± 0.14	1491
				U	L				
			U	70	30				
			L	5	95				
	SNV + 1st derivative	Actual	Predicted			93 ± 3	0.89	0.64 ± 0.13	1491
				U	L				
			U	70	30				
			L	5	95				
Vis-NIR (380-2470 nm)	Raw data	Actual	Predicted			91 ± 5	0.72	0.47 ± 0.10	2336
				U	L				
			U	44	56				
			L	5	95				
	SNV	Actual	Predicted			92 ± 4	0.73	0.51 ± 0.12	1147
				U	L				
			U	46	54				
			L	4	96				
	1st derivative	Actual	Predicted			88 ± 8	0.63	0.40 ± 0.09	998
				U	L				
			U	44	56				
			L	8	92				
	1st derivative + SNV	Actual	Predicted			88 ± 4	0.64	0.38 ± 0.07	998
				U	L				
			U	43	57				
			L	8	92				
	SNV + 1st derivative	Actual	Predicted			88 ± 5	0.65	0.37 ± 0.07	977
				U	L				
			U	43	57				
			L	8	92				

Table 5
Twenty most relevant wavelengths of the best obtained classification models for each mycotoxin and equipment using a soft-voting ensemble classifier (logistic regression + partial least squares (PLS) regression).

Mycotoxin	Equipment	Pre-treatment	20 most relevant wavelengths (nm)
DON	NIR-HSI (1000-1600 nm)	1st derivative + SNV	1491, 1486, 1312, 1247, 1343, 1252, 1409, 1404, 1399, 1429, 1383, 1267, 1544, 1575, 1198, 1539, 1518, 1533, 1052, 1272
		SNV + 1st derivative	1312, 1486, 1491, 1343, 1544, 1198, 1429, 1383, 1378, 1575, 1481, 1252, 1434, 1409, 1404, 1368, 1533, 1203, 1358, 1528
	Vis-NIR (380-2470 nm)	Raw data	2336, 456, 2405, 2335, 442, 423, 2355, 411, 465, 2356, 2404, 2385, 414, 2462, 412, 441, 449, 417, 422, 2400
		SNV	417, 399, 407, 1144, 1145, 1147, 1146, 1205, 1206, 991, 411, 1097, 999, 400, 1143, 1204, 1139, 1148, 465, 1138
ZEN	NIR-HSI (1000-1600 nm)	SNV	1193, 1523, 1481, 1502, 1287, 1173, 1096, 1247, 1282, 1144, 1533, 1237, 1491, 1554, 1292, 1232, 1178, 1419, 1337, 1429
		1st derivative + SNV	1277, 1282, 1105, 1544, 1110, 1272, 1409, 1297, 1491, 1188, 1363, 1257, 1267, 1549, 1091, 1237, 1554, 1086, 1414, 1404
	Vis-NIR (380-2470 nm)	Raw data	2360, 2391, 2359, 423, 2403, 440, 2392, 2402, 2361, 2283, 424, 457, 2390, 2362, 2470, 2439, 456, 2282, 2445, 476
		SNV	1121, 1135, 1101, 1136, 2391, 1201, 1120, 1100, 1119, 1198, 1118, 397, 1180, 1102, 384, 393, 1206, 1122, 414, 398
DON + ZEN	NIR-HSI (1000-1600 nm)	SNV	1481, 1282, 1353, 1497, 1581, 1378, 1419, 1523, 1149, 1272, 1570, 1125, 1414, 1287, 1247, 1292, 1057, 1188, 1096, 1491
		SNV + 1st derivative	1491, 1486, 1343, 1544, 1378, 1312, 1383, 1429, 1272, 1575, 1277, 1358, 1198, 1368, 1373, 1481, 1252, 1528, 1267, 1434
	Vis-NIR (380-2470 nm)	Raw data	**2336, 2335, 2405, 2404, 435, 2355, 456, 2400, 2392, 998, 999, 422, 2391, 2350, 2369, 2401, 2368, 2374, 2460, 991**
		SNV	1147, 1205, 991, 399, 1206, 2336, 1204, 979, 1146, 417, 999, 1444, 407, 465, 2335, 998, 1148, 980, 966, 1145

key spectral ranges. This indicates that the combined model does not rely on fundamentally different spectral information but rather exploits complementary wavelengths within established *Fusarium*-sensitive regions to identify grains contaminated by either mycotoxin.

Importantly, the practical benefits of this combined classification approach extend beyond accurate prediction. By applying this model, it would be possible to significantly reduce the concentration of multiple mycotoxins within a single step. As shown, the removal of grains exceeding both legal limits could reduce the mean DON concentration by 89.5%, 98.1% for DON-3G, 95.2% for 15-ADON, 95.7% for 3-ADON, and 67.0% for ZEN levels. From an industrial perspective, this combined DON + ZEN classification strategy is particularly attractive. Simultaneous identification using a single decision step reduces system complexity compared with deploying separate classifiers for each toxin and facilitates integration into real-time sorting lines. Importantly, the combined models showed prediction times and throughput comparable to those of the individual DON and ZEN models, indicating that the expanded detection capability does not impose a computational penalty. As a result, the DON + ZEN model offers an efficient and scalable solution for high-throughput grain sorting systems, where robustness, simplicity and processing speed are critical. However, future research should address the current imbalance in the distribution of contaminated and non-contaminated grains. The scarcity of naturally occurring highly contaminated grains presents a challenge and limits the robustness of models. Expanding datasets to include a broader range of contamination levels, particularly grains above regulatory thresholds, would help validate models under more realistic conditions and improve their generalisation across oat varieties and environments.

3.7. Multispectral classification models

The selection of the most relevant wavelengths is a critical step in simplifying spectroscopic models and enhancing their applicability in real-time, industrial environments (Wan et al., 2020). For this reason, the two best models for each mycotoxin or mycotoxin combination (DON, ZEN, and DON + ZEN), and for each equipment (NIR-HSI and Vis-NIR), were selected and used to extract the 20 most influential wavelengths (Table 5). These wavelengths were then used to redefine the classification models using a reduced spectral input in a multispectral configuration. The results of these new models are presented in Table 6.

In addition, further dimensionality reduction was explored by retraining the same models using only the top 10 and top 5 wavelengths. While these configurations offered additional simplification from a hardware perspective, they generally resulted in a clear decrease in F1-score and CA, together with increased variability across cross-validation folds. Consequently, these configurations were considered less robust for reliable identification of highly contaminated grains and were not retained for further analysis.

For NIR-HSI, wavelength reduction to 20 spectral bands did not compromise classification performance and, in some cases, slightly improved it. For DON classification, multispectral models achieved CAs of 94 ± 4% and 95 ± 3%, respectively, with F1-scores of 0.66-0.67. These results are comparable to, or marginally higher than, those obtained with the corresponding full-spectrum models, demonstrating that the most informative spectral information is effectively preserved within a limited number of wavelengths. Similarly, for ZEN classification, multispectral models performed exceptionally well. The SNV model achieved a CA of 98 ± 2% (F1-score = 0.72 ± 0.24), while the 1st derivative + SNV model reached 99 ± 1% CA (F1-score = 0.95 ± 0.11), closely matching the near-perfect performance observed with full-spectrum data. For the combined DON + ZEN classification, multispectral NIR-HSI models yielded CAs of 93 ± 4% and 92 ± 7%, with stable F1-scores around 0.63-0.66.

In contrast, wavelength reduction had a more pronounced negative effect on Vis-NIR classification performance. For DON, the multispectral Vis-NIR models showed a clear decrease in both CA and F1-score compared with their full-spectrum counterparts. A similar trend was observed for ZEN and DON + ZEN classifications, where multispectral Vis-NIR models exhibited lower accuracies and increased variability. This behaviour reflects the intrinsic differences between the two techniques. Vis-NIR spectroscopy relies on point-based measurements, which are more sensitive to local heterogeneity, grain orientation and surface effects. Consequently, full-spectrum models benefit from spectral redundancy that helps compensate for local variability. When the spectral input is restricted to a limited number of wavelengths, this redundancy is reduced, leading to a loss of robustness.

From an industrial implementation perspective, these findings highlight a clear distinction between the two spectroscopic techniques. NIR-HSI is particularly well suited to multispectral implementations. This inherent spatial averaging enables reliable classification even when the spectral input is reduced to a limited number of wavelengths, making multispectral NIR-HSI highly attractive for real-time grain sorting applications, such as conveyor-belt systems where large numbers

Table 6
Classification accuracies (CAs), F-1 score and confusion for validation sets in the classification of oat grains with redefined models using the 20 most relevant wavelengths according to the European Union (EU) legal limit for deoxynivalenol (DON) (1750 μg/kg) and zearalenone (ZEN) (100 μg/kg), obtained using a soft-voting ensemble classifier (logistic regression + partial least squares (PLS) regression). U = grains above the thresholds; L = grains below the thresholds; SD = standard deviation.

Mycotoxin	Equipment	Pre-treatment	Confusion matrix (%)				CA (%) ± SD	F1-score ± SD
DON	NIR-HSI (1000-1600 nm)	1st derivative + SNV	Actual	Predicted			94 ± 4	0.66 ± 0.15
					U	L		
				U	71	29		
				L	4	96		
		SNV + 1st derivative	Actual	Predicted			95 ± 3	0.67 ± 0.13
					U	L		
				U	69	31		
				L	3	97		
	Vis-NIR (380-2470 nm)	Raw data	Actual	Predicted			60 ± 26	0.25 ± 0.06
					U	L		
				U	71	29		
				L	41	59		
		SNV	Actual	Predicted			86 ± 9	0.39 ± 0.10
					U	L		
				U	48	52		
				L	10	90		
ZEN	NIR-HSI (1000-1600 nm)	SNV	Actual	Predicted			98 ± 2	0.72 ± 0.24
					U	L		
				U	83	17		
				L	2	98		
		1st derivative + SNV	Actual	Predicted			99 ± 1	0.95 ± 0.11
					U	L		
				U	100	0		
				L	1	99		
	Vis-NIR (380-2470 nm)	Raw data	Actual	Predicted			82 ± 22	0.41 ± 0.30
					U	L		
				U	92	8		
				L	18	82		
		SNV	Actual	Predicted			88 ± 21	0.53 ± 0.33
					U	L		
				U	92	8		
				L	12	88		
DON + ZEN	NIR-HSI (1000-1600 nm)	SNV	Actual	Predicted			93 ± 4	0.63 ± 0.13
					U	L		
				U	60	40		
				L	3	97		
		SNV + 1st derivative	Actual	Predicted			92 ± 7	0.66 ± 0.18
					U	L		
				U	72	28		
				L	6	94		
	Vis-NIR (380-2470 nm)	Raw data	Actual	Predicted			85 ± 20	0.44 ± 0.14
					U	L		
				U	46	54		
				L	12	88		
		SNV	Actual	Predicted			86 ± 14	0.46 ± 0.14
					U	L		
				U	56	44		
				L	11	89		

of grains must be assessed rapidly and consistently. In contrast, although Vis-NIR spectroscopy remains appealing due to its lower cost and simpler hardware configuration, its classification performance in this study was more strongly dependent on full-spectrum information, and even under these conditions its performance remained substantially lower than that achieved with NIR-HSI. Taken together, these results support multispectral NIR-HSI as a robust and efficient compromise between classification performance, computational efficiency and industrial feasibility. While Vis-NIR may remain suitable for low-cost screening applications, multispectral NIR-HSI offers a more favourable cost-benefit balance when robustness and reliability at industrial throughput are prioritised.

From a computational perspective, restricting the input from full-spectrum data to the top 20 selected wavelengths resulted in small but consistent changes in computation time across configurations. For most of the best-performing models, the reduction in inference time per spectrum was modest (typically 0-2%), while in the most favourable case a reduction of approximately 20% was observed (e.g., ZEN classification using NIR-HSI with 1st derivative + SNV preprocessing, 7.4 to 5.9 μs). It should be noted that these timings were measured on a standard workstation under non-controlled conditions and therefore should be interpreted as indicative rather than absolute. In practical

sorting lines, this transition to multispectral models significantly enhances their feasibility. Reducing the number of wavelengths from hundreds or thousands to 20 substantially decreases data dimensionality, processing requirements, and hardware complexity. Notably, overall throughput is often dominated by spectral acquisition, illumination, and data transfer rather than classifier inference time alone. Consequently, wavelength reduction primarily facilitates hardware implementation and acquisition speed rather than further reductions in computation time.

These findings support the deployment of targeted multispectral sensors for mycotoxin detection, offering a promising route to reduce the risk of contaminated batches entering the food chain. The demonstrated robustness of the 20-wavelength NIR-HSI models highlights the strong potential of this approach.

4. Conclusions

This study demonstrates that spectroscopic techniques can be effectively applied for the detection of individual oat grains contaminated with DON, its modified forms (DON-3G, 3-ADON and 15-ADON), and ZEN. Overall, NIR-HSI clearly outperformed Vis-NIR spectroscopy, providing consistently higher CA and F1-scores, as well as greater robustness across all contamination scenarios.

Classification models based on NIR-HSI achieved excellent performance, particularly when appropriate spectral pre-treatments were applied. The most informative spectral information was consistently located in the NIR regions 1000-1250 nm and 1300-1500 nm, which were identified as relevant across all toxins and classification tasks. These regions are associated with indirect biochemical and structural changes induced by *Fusarium* infection, likely affecting hull structure, protein composition and fibre content rather than reflecting direct absorption by the mycotoxins themselves.

Models combining DON and ZEN detection enabled simultaneous removal of grains contaminated with multiple mycotoxins, offering a practical 2-in-1 solution. Applying this combined model could lead to substantial reductions in overall toxin concentrations, particularly for DON and its modified forms.

From an applied perspective, the results highlight the advantage of selectively removing a small fraction of highly contaminated grains, which are primarily responsible for batch non-compliance. Such targeted screening strategies can prevent unnecessary rejection of entire oat batches, thereby enhancing food safety and regulatory compliance while improving sustainability and economic efficiency within cereal processing chains.

Nevertheless, addressing the current class imbalance and expanding datasets with naturally contaminated grains would further improve model robustness and applicability.

CRediT authorship contribution statement

Irene Teixido-Orries: Writing – original draft, Visualization, Validation, Software, Methodology, Investigation, Formal analysis, Data curation, Conceptualization. **Francisco Molino:** Writing – review & editing, Writing – original draft, Supervision, Project administration, Methodology, Investigation, Data curation, Conceptualization. **Carol Verheecke-Vaessen:** Writing – review & editing, Writing – original draft, Supervision, Methodology, Investigation, Funding acquisition, Data curation, Conceptualization. **Angel Medina:** Supervision, Project administration. **Sonia Marín:** Writing – review & editing, Writing – original draft, Supervision, Project administration, Methodology, Funding acquisition, Conceptualization.

Declaration of competing interest

The authors declare that they have no known competing financial interests or personal relationships that could have appeared to influence the work reported in this paper.

Acknowledgements

This work was supported by the Spanish Ministry of Science and Innovation (predoctoral grant FPU21/00073 and Project PID2020-114836RB-I00 funded by MCIN/AEI/10.13039/501100011033) and Cranfield University. We thank Dr. Thomas Börjesson and Agroväst Livsmedel AB for providing oat samples. We also acknowledge the technical help of Monika Jodkowska in the analysis of the experiment. We are grateful to Pau Agusti-Fernandez for his valuable support and advice in data analysis.

Appendix A. Supplementary data

Supplementary data to this article can be found online at https://doi.org/10.1016/j.foodcont.2026.112033.

Data availability

Data will be made available on request.

References

Badr Eldin, A. (2010). Near-infrared spectroscopy. *Pharmacopeial Forum, 36*(2), 532. https://doi.org/10.5772/24208

Barbedo, J. G. A., Tibola, C. S., & Lima, M. I. P. (2017). Deoxynivalenol screening in wheat kernels using hyperspectral imaging. *Biosystems Engineering, 155*, 24–32. https://doi.org/10.1016/j.biosystemseng.2016.12.004

Bezerra da Rocha, M. E., da Chagas Oliveira, F. F., Feitosa Maia, F. E., Florindo Guedes, M. I., & Rondina, D. (2014). Mycotoxins and their effects on human and animal health. *Food Control, 36*(1), 159–165. https://doi.org/10.1016/j.foodcont.2013.08.021

Blackshaw-Crosby, J. R. (2021). *Investigating Fusarium resistance in UK winter oats*. Harper Adams University.

Chavez, R. A., Cheng, X., & Stasiewicz, M. J. (2020). A review of the methodology of analyzing aflatoxin and fumonisin in single corn kernels and the potential impacts of these methods on food security. *Foods, 9*(3). https://doi.org/10.3390/foods9030297

Delwiche, S. R., Rodriguez, I. T., Rausch, S. R., & Graybosch, R. A. (2019). Estimating percentages of *Fusarium*-damaged kernels in hard wheat by near-infrared hyperspectral imaging. *Journal of Cereal Science, 87*, 18–24. https://doi.org/10.1016/j.jcs.2019.02.008

Dropa, T., Dzuman, Z., & Jonatova, P. (2021). Mycotoxins in oat flakes – Changes during production and occurrence on the Czech market. *Czech Journal of Food Sciences, 39*(2), 131–139. https://doi.org/10.17221/247/2020-CJFS

Ekwomadu, T. I., Akinola, S. A., & Mwanza, M. (2021). *Fusarium* mycotoxins, their metabolites (Free, emerging, and masked), food safety concerns, and health impacts. *International Journal of Environmental Research and Public Health, 18*(22). https://doi.org/10.3390/ijerph182211741

European Commission. (2023a). Commission implementing regulation (EU) 2023/2782 of 14 December 2023 laying down the methods of sampling and analysis for the control of the levels of mycotoxins in food and repealing Regulation (EC) no 401/2006. *Official Journal of the European Union*, 1–44.

European Commission. (2023b). Commission Regulation (EU) 2023/915 of 25 April 2023 on maximum levels for certain contaminants in food and repealing Regulation (EC) no 1881/2006. *Official Journal of the European Union, 119*, 103–157.

European Commission. (2024a). Commission Regulation (EU) 2024/1022 of 8 April 2024 amending Regulation (EU) 2023/915 as regards maximum levels of deoxynivalenol in food. *Official Journal of the European Union L*, 1–4. https://doi.org/10.2903/j.efsa.2017.4718

Femenias, A., Bainotti, M. B., Gatius, F., Ramos, A. J., & Marín, S. (2021). Standardization of near infrared hyperspectral imaging for wheat single kernel sorting according to deoxynivalenol level. *Food Research International, 139*. https://doi.org/10.1016/j.foodres.2020.109925

Femenias, A., Gatius, F., Ramos, A. J., Sanchis, V., & Marín, S. (2020). Use of hyperspectral imaging as a tool for *Fusarium* and deoxynivalenol risk management in cereals: A review. *Food Control, 108*. https://doi.org/10.1016/j.foodcont.2019.106819

Femenias, A., Gatius, F., Ramos, A. J., Teixido-Orries, I., & Marín, S. (2022). Hyperspectral imaging for the classification of individual cereal kernels according to fungal and mycotoxins contamination: A review. *Food Research International, 155*. https://doi.org/10.1016/j.foodres.2022.111102

Femenias, A., Llorens-Serentill, E., Ramos, A. J., Sanchis, V., & Marín, S. (2022). Near-infrared hyperspectral imaging evaluation of *Fusarium* damage and DON in single wheat kernels. *Food Control, 142*. https://doi.org/10.1016/j.foodcont.2022.109239

Fredlund, E., Gidlund, A., Sulyok, M., Börjesson, T., Krska, R., Olsen, M., & Lindblad, M. (2013). Deoxynivalenol and other selected *Fusarium* toxins in Swedish oats - Occurrence and correlation to specific *Fusarium* species. *International Journal of Food Microbiology, 167*(2), 276–283. https://doi.org/10.1016/j.ijfoodmicro.2013.06.026

Freitag, S. (2025). Infrared spectroscopy for mycotoxin screening: Advantages and limitations. In *Mycotoxins: Screening and confirmatory analysis* (pp. 249–266). Wageningen, The Netherlands: Wageningen Academic Publishers. https://doi.org/10.1163/9789004724969_012.

Hofgaard, I. S., Aamot, H. U., Torp, T., Jestoi, M., Lattanzio, V. M. T., Klemsdal, S. S., Waalwijk, C., Van Der Lee, T., & Brodal, G. (2016). Associations between *Fusarium* species and mycotoxins in oats and spring wheat from farmers fields in Norway over a six-year period. *World Mycotoxin Journal, 9*(3), 365–378. https://doi.org/10.3920/WMJ2015.2003

Krska, R., Malachova, A., Berthiller, F., & Van Egmond, H. P. (2014). Determination of T-2 and HT-2 toxins in food and feed: An update. *World Mycotoxin Journal, 7*(2), 131–142. https://doi.org/10.3920/WMJ2013.1605

Maphaisa, T. C., Akinmoladun, O. F., Adelusi, O. A., Mwanza, M., Fon, F., Tangni, E., & Njobeh, P. B. (2025). Advances in mycotoxin detection techniques and the crucial role of reference material in ensuring food safety. A review. *Food and Chemical Toxicology, 200*. https://doi.org/10.1016/j.fct.2025.115387

Martin, C., Schöneberg, T., Vogelgsang, S., Mendes Ferreira, C. S., Morisoli, R., Bertossa, M., Bucheli, T. D., Mauch-Mani, B., & Mascher, F. (2018). Responses of oat grains to *Fusarium poae* and *F. langsethiae* infections and mycotoxin contaminations. *Toxins, 10*(1). https://doi.org/10.3390/toxins10010047

Martinelli, J. A., Soares Chaves, M., Sganzerla Graichen, F. A., Carlos Federizzi, L., & Felipe Dresch, L. (2014). Impact of fusarium head blight in reducing the weight of oat grains. *Journal of Agricultural Science, 6*(5). https://doi.org/10.5539/jas.v6n5p188

Meenu, M., Zhang, Y., Kamboj, U., Zhao, S., Cao, L., He, P., & Xu, B. (2022). Rapid determination of β-glucan content of hulled and naked oats using near infrared spectroscopy combined with chemometrics. *Foods, 11*(1). https://doi.org/10.3390/foods11010043

Meyer, J. C., Hennies, I., Wessels, D., & Schwarz, K. (2021). Survey of mycotoxins in milling oats dedicated for food purposes between 2013 and 2019 by LC–MS/MS. *Food Additives & Contaminants Part A Chemistry, Analysis, Control, Exposure and Risk Assessment, 38*(11), 1934–1947. https://doi.org/10.1080/19440049.2021.1950931

Nathanail, A. V., Syvähuoko, J., Malachová, A., Jestoi, M., Varga, E., Michlmayr, H., Adam, G., Sieviläinen, E., Berthiller, F., & Peltonen, K. (2015). Simultaneous determination of major type A and B trichothecenes, zearalenone and certain modified metabolites in Finnish cereal grains with a novel liquid chromatography-tandem mass spectrometric method. *Analytical and Bioanalytical Chemistry, 407*(16), 4745–4755. https://doi.org/10.1007/s00216-015-8676-4

Ning, H., Wang, J., Jiang, H., & Chen, Q. (2022). Quantitative detection of zearalenone in wheat grains based on near-infrared spectroscopy. *Spectrochimica Acta - Part A: Molecular and Biomolecular Spectroscopy, 280*. https://doi.org/10.1016/j.saa.2022.121545

Paudel, D., Dhungana, B., Caffe, M., & Krishnan, P. (2021). A review of health-beneficial properties of oats. *Foods, 10*(11). https://doi.org/10.3390/foods10112591

Redaelli, R., & Berardo, N. (2002). Evaluation of groat percentage in oats (*Avena sativa* L.) by near infrared spectroscopy. *Journal of Near Infrared Spectroscopy, 10*(2), 103–109. https://doi.org/10.1255/jnirs.327

Rychlik, M., Humpf, H. U., Marko, D., Dänicke, S., Mally, A., Berthiller, F., Klaffke, H., & Lorenz, N. (2014). Proposal of a comprehensive definition of modified and other forms of mycotoxins including "masked" mycotoxins. *Mycotoxin Research, 30*(4), 197–205. https://doi.org/10.1007/s12550-014-0203-5

Serranti, S., Cesare, D., Marini, F., & Bonifazi, G. (2013). Classification of oat and groat kernels using NIR hyperspectral imaging. *Talanta, 103*, 276–284. https://doi.org/10.1016/j.talanta.2012.10.044

Tarazona, A., Gómez, J. V., Mateo, F., Jiménez, M., & Mateo, E. M. (2021). Potential health risk associated with mycotoxins in oat grains consumed in Spain. *Toxins, 13*(6). https://doi.org/10.3390/toxins13060421

Taylor, M. E., & Newkirk, R. W. (2023). Sorting capability and grain recovery of deoxynivalenol contaminated wheat is affected by calibration and vitreous kernel settings from near-infrared transmittance technology. *World Mycotoxin Journal, 16*(1), 49–57. https://doi.org/10.3920/WMJ2021.2751

Teixido-Orries, I., Molino, F., Agusti-Fernandez, P., Ayibiowu, E., Croucher, D., Medina, A., Marín, S., & Verheecke-Vaessen, C. (2026). Visible-near infrared spectroscopy and near-infrared hyperspectral imaging for the detection of T-2 and HT-2 toxins in individual oat grains. *Food Control, 180*. https://doi.org/10.1016/j.foodcont.2025.111676

Teixido-Orries, I., Molino, F., Castro-Criado, B., Jodkowska, M., Medina, A., Marín, S., & Verheecke-Vaessen, C. (2025). Mapping variability of mycotoxins in individual oat kernels from batch samples: Implications for sampling and food safety. *Toxins, 17*(1). https://doi.org/10.3390/toxins17010034

Teixido-Orries, I., Molino, F., Femenias, A., Ramos, A. J., & Marín, S. (2023). Quantification and classification of deoxynivalenol-contaminated oat samples by near-infrared hyperspectral imaging. *Food Chemistry*. , Article 135924. https://doi.org/10.1016/j.foodchem.2023.135924

Teixido-Orries, I., Molino, F., Gatius, F., Sanchis, V., & Marín, S. (2023). Near-infrared hyperspectral imaging as a novel approach for T-2 and HT-2 toxins estimation in oat samples. *Food Control, 153*. https://doi.org/10.1016/j.foodcont.2023.109952

Teixido-Orries, I., Yang, L., Molino, F., Medina, A., Marín, S., & Verheecke-Vaessen, C. (2025). Detection of *Fusarium* spp. and T-2 and HT-2 toxins contamination in oats using visible and near-infrared spectroscopy. *International Journal of Food Microbiology, 441*. https://doi.org/10.1016/j.ijfoodmicro.2025.111301

Tekle, S., Bjørnstad, Å., Skinnes, H., Dong, Y., & Segtnan, V. H. (2013). Estimating deoxynivalenol content of ground oats using VIS-NIR spectroscopy. *Cereal Chemistry, 90*(3), 181–185. https://doi.org/10.1094/CCHEM-07-12-0084-R

Tekle, S., Mage, I., Segtnan, V. H., & Bjornstad, A. (2015). Near-infrared hyperspectral imaging of *Fusarium*-damaged oats (*Avena sativa* L.). *Cereal Chemistry, 92*(1), 73–80. https://doi.org/10.1094/CCHEM-04-14-0074-R

Walsh, K. B., Blasco, J., Zude-Sasse, M., & Sun, X. (2020). Visible-NIR 'point' spectroscopy in postharvest fruit and vegetable assessment: The science behind three decades of commercial use. *Postharvest Biology and Technology, 168*. https://doi.org/10.1016/j.postharvbio.2020.111246

Wan, G., Liu, G., He, J., Luo, R., Cheng, L., & Ma, C. (2020). Feature wavelength selection and model development for rapid determination of myoglobin content in nitrite-cured mutton using hyperspectral imaging. *Journal of Food Engineering, 287*. https://doi.org/10.1016/j.jfoodeng.2020.110090

Wenzl, T., Robouch, P., Schaechtele, A., Haedrich, J., Stroka, J., & European Commission. Joint Research Centre. (2016). *Guidance document on the estimation of LOD and LOQ for measurements in the field of contaminants in feed and food.* Publications Office.

Yan, W., Pageau, D., Martin, R., Cummiskey, A., & Blackwell, B. (2017). Is deoxynivalenol contamination a serious problem for oat in eastern Canada? *Crop Science, 57*(1), 88–98. https://doi.org/10.2135/cropsci2016.04.0263

Yang, Z., Xie, C., Bao, Y., Liu, F., Wang, H., & Wang, Y. (2023). Oat: Current state and challenges in plant-based food applications. *Trends in Food Science and Technology, 134*, 56–71. https://doi.org/10.1016/j.tifs.2023.02.017

Zareef, M., Arslan, M., Hassan, M. M., Ahmad, W., Ali, S., Li, H., Ouyang, Q., Wu, X., Hashim, M. M., & Chen, Q. (2021). Recent advances in assessing qualitative and quantitative aspects of cereals using nondestructive techniques: A review. *Trends in Food Science and Technology, 116*, 815–828. https://doi.org/10.1016/j.tifs.2021.08.012

https://dspace.org/

Detection of deoxynivalenol, its modified forms, and zearalenone in individual oat grains using visible-near-infrared spectroscopy and near-infrared hyperspectral imaging

Teixido-Orries, Irene; Molino, Francisco; Verheecke-Vaessen, Carol; Medina, Angel; Marín, Sonia

2026-06
Elsevier
https://doi.org/10.1016/j.foodcont.2026.112033
Teixido-Orries I, Molino F, Verheecke-Vaessen C, et al., (2026) Detection of deoxynivalenol, its modified forms, and zearalenone in individual oat grains using visible-near-infrared spectroscopy and near-infrared hyperspectral imaging. Food Control, Volume 184, June 2026, Article number 112033

Downloaded from a DSpace repository. https://dspace.org/